RSC Advances

ROYAL SOCIETY OF CHEMISTRY

www.rsc.org/advances

Synthesis, characterization and biological evaluation of *N*-(2,3-dimethyl-5-oxo-1-phenyl-2,5-dihydro-1*H*-pyrazol-4-yl)benzamides

Aamer Saeed[a*], Syeda Abida Ejaz[b], Asma Khurshid[a], Sidra Hassan[b], Mariya al-Rashida[c], Muhammad Latif[d], Joanna Lecka[e,f], Jean Sévigny[e,f] & Jamshed Iqbal[b*]

[a] *Department of Chemistry, Quaid-I-Azam University, 45320, Islamabad, Pakistan*

[b]*Centre for Advanced Drug Research, COMSATS Institute of Information Technology, Abbottabad 22060, Pakistan*

[c]*Department of Chemistry, Forman Christian College (A Chartered University), Ferozepur Road-54600, Lahore, Pakistan*

[d]*Medicinal/Pharmaceutical Chemistry Laboratory,Korea Research Institute of Chemical Technology 141-Gajeongro, Yuseong, Daejeon 305-600, South Korea.*

[e] *Département de microbiologie-infectiologie et d'immunologie, Faculté de Médecine, Université Laval, Québec, QC, Canada*

[f] *Centre de Recherche du CHU de Québec – Université Laval, Québec, QC, Canada*

To whom Correspondence should address:

Prof. Dr. Jamshed Iqbal

Centre for Advanced Drug Research, COMSATS Institute of Information Technology, Abbottabad 22060, Pakistan.

Tel.: +92 992 383591 96; Fax: +92 992 383441. E-mail addresses: drjamshed@ciit.net.pk

[*] Email: aamersaeed@yahoo.com, Tel +92-51-9064-2128; Fax: +92-51-9064-2241

Abstract:

We report the synthesis of a series of different substituted *N*-(2,3-dimethyl-5-oxo-1-phenyl-2,5-dihydro-1*H*-pyrazol-4-yl)benzamides by making use of a non-steroidal anti-inflammatory drug

known as 4-aminophenazone also called as antipyrine, a compound of great interest in drug chemistry. These compounds possess potential biological applications and were screened against human recombinant alkaline phosphatase including human tissue-nonspecific alkaline phosphatase (*h*-TNAP), tissue specific human intestinal alkaline phosphatase (*h*-IAP), human placental alkaline phosphatase (*h*-PLAP) and human germ cell alkaline phosphatase (*h*-GCAP). These compounds were also tested for their inhibitory potential against recombinant human and rat ecto-5'-nucleotidases (*h*-e5-NT & *r*-e5-NT, respectively). All benzamide derivatives inhibited APs to a lesser degree than e5-NT. The reported compounds are of considerable interest for further applications in the field of medicinal chemistry as these compounds have potential to bind nucleotide protein targets.

Keywords: alkaline phosphatase, antipyrine, human recombinant, human Germ cell, intestinal alkaline phosphatase

Introduction

Ecto-nucleotidases enzymes are subdivided into four major families: the ecto-nucleoside 5′-triphosphate diphosphohydrolases (NTPDases), the alkaline phosphatases (APs), the ecto-nucleotide pyrophosphatases (NPPs) and the ecto-5′-nucleotidases (e5NT).[1] These enzymes are responsible for the hydrolysis of a wide range of extracellular nucleotides to nucleosides and adenosine.[2] Adenosine monophosphate (AMP) is a significant biological substrate of ecto-5'-nucleotidase as its hydrolysis produces adenosine, which acts on P_1 receptors.[3] AMP is produced by the degradation of P_2 receptor agonists ATP and ADP by the other ectonucleotidases mentioned above. Among the different nucleotidases, ecto-5'-nucleotidase is expressed by several cells including by those localized on the outer surface of endothelial cells of large and small arteries. Hypoxia increases the expression of ecto-5'-nucleotidase and it is generally up-regulated at the site of inflammation.[4]

Alkaline phosphatases are the other important enzymes for the production of adenosine either directily by the conversion of adenosine monophosphate (AMP) into adenosine (Ado) or indirectly by the conversion of ATP → ADP which is then converted to AMP and finally to Ado.[5] AP hydrolyzes a variety of substrates other than nucleotides, such as bis(p-nitrophenyl)phosphate, inorganic polyphosphates, phosphatidates and glucose-phosphates.[6] In

the presence of large concentrations of phosphate acceptors, these APs are also responsible for catalyzing various transphosphorylation reactions. In humans, there are four AP isozymes. Three of these are tissue specific enzymes, i.e. germ cell AP (GCAP), placental AP (PLAP) and intestinal AP (IAP). They have relative homologies in the range of 90–98% and their genes are clustered on chromosome 2. The fourth (tissue-nonspecific AP; TNAP) is found in liver, kidney and most abundantly in bones.[7] The gene of TNAP is located on chromosome 1 and it is only 50% identical to the other three isozymes. TNAP has various functions depending of the tissue where it is expressed. An important role demonstrated for this enzyme is to hydrolyze a potent calcification inhibitor, inorganic pyrophosphate.[8] The intestinal alkaline phosphatase is found at the brush boarder of the intestinal epithelium and enriched in surfactant-like particles (SLP). They are likely to be involved in intestinal absorption of the lipid/nutrients across the cell membrane via its association with SLP. Because of a high homology between TNAP and tissue-specific IAP, very few selective inhibitors of IAP have been reported.[9] The tissue-specific placental alkaline phosphatase (PLAP) is highly expressed in placental tissue and its biological function is still unknown.[10] The PLAP-like enzymes are observed in serum of patients with primary testicular tumors, in particular seminoma[11] and other cancers.[12] PLAP and GCAP are often co-expressed in ovarian cancers and it has been reported that transformation from normal to malignant trophoblast might be associated with a switch from PLAP to GCAP expression.[3]

We report here various benzamide derivatives containing pyrazole as excellent inhibitors of e5-NT and alkaline phosphatases (*h*-TNAP,*h*- IAP, *h*-PLAP and *h*-GCAP). Some of the compounds were found to be more selective as inhibitors of e5-NT even at lower concentrations and can be developed further to synthesize even more potent and selective compounds lead derivatives.

Aminophenazone is one of the antipyrine derivatives which was first synthesized by Knorr in 1833 and ever since the antipyrine derivatives (APDs) have been studied. The antipyrine derivatives have been investigated in a variety of fields.[13] The nonlinear optical and UV-vis studies indicate that these antipyrine derivatives are the promising photo electronic materials. Aminophenazone derivatives have been shown to possess a number of potent biological applications including their use as antipyretic, analgesic and anti-inflammatory agents.[14] The presence of amide linkage imparts useful biological applications to aminophenazone moiety. Since amides are an important class of organic compounds and can be synthesized in a number of ways either by direct coupling of carboxylic acids and amines at high temperatures or through

microwave assisted methodologies and even through organo catalysts. The exploration of amidic linkage in various drugs has far more enhanced the importance of amides and has broadened the scope of their biological applications like anthelmintic, antihistamine, antifungal, and antibacterial etc.[15] Both alkaline phosphatase (AP) and ecto-5′-nucleotidase (e5NT) are responsible for hydrolyzing nucleotides. AP is substrate non-specific and is a major enzyme responsible for AMP hydrolysis (although it hydrolysis other nucleotides as well), on the other hand ecto-5-nucleotidase is a substrate specific enzyme and only hydrolyzes AMP to adenosine with the release of phosphate group[16,17]. Pyrazole derivatives have previously been identified as inhibitors of AP[18], keeping this in mind our research group focused on design of new pyrazole derivatives containing amide linkages as potential inhibitors of AP, since e5NT is also a major AMP hydrolyzing enzyme, therefore activity against this enzyme was also evaluated.

Experimental Section

Melting points were determined using Gallenkamp melting point apparatus (MP-D) and are uncorrected. Infrared spectra were recorded using a Shimadzu IR 460 as KBr pellets. ^{1}H-NMR spectra were obtained using a Bruker 300 NMR MHz spectrometer in $CDCl_3$ solution using TMS as an internal reference. ^{13}CNMR spectra were obtained by (75 MHz) NMR spectrometer in deuterated solvents. Thin layer chromatography was performed on pre-coated silica gel aluminum plates (layer thickness 0.2 mm, HF 254, Reidal-de-Haen from Merck). Chromatogram was detected by using ultraviolet light (254 and 260nm). MS were recorded using an EI source of (70 EV) on Agilent Technologies 6890N (GC) and an inert mass selective detector 5973 mass spectrometer.

General procedure for the synthesis of *N*-(1,5-Dimethyl-3-oxo-2-phenyl-2,3-dihydro-1*H*-pryazole-4-yl)benzamide (4a):

Brownish black amorphous solid; Yield; 89%, m.p: 133-134 °C; IR (neat): 3140 (CO**NH**), 2967, 2829, (Csp^3-H), 1677 (**CO**NH), 1421, 1340 (Csp^3-H bending): ^{1}H-NMR ($CDCL_3$, 300MHz): δ 8.09 (m, 5H, Ar-H, s, 1H, N-H), 7.84 (m, 4H, Ar-H), 3.07 (s, 3H), 2.10 (s, 3H); ^{13}C-NMR ($CDCL_3$, 75MHz): δ 173.02 (**CO**NH), 170.89 (-C=C-**CO**-N-), 161.45, 152.28, 134.67, 133.46, 132.33, 130.10, 129.72, 129.31, 128.46, 127.47, 124.77,35.36 (**CH_3**-N-), 10.62 (**CH_3**-C_{SP}^2-), 12.78 (**CH_3**-Ar-C).LC-MS (m/z) %: M^+ 308, 214, 203. Elemental analysis found $C_{18}H_{17}N_3O_2$: C 69.00, H 6.92, N 12.05.

***N*-(1,5-Dimethyl-3-oxo-2-phenyl-2,3-dihydro-1*H*-pryazole-4-yl)-2-methylbenzamide (4b):**

Brown amorphous solid; Yield; 86%, m.p: 125-126 °C; IR (neat): 3150 (CO**NH**), 2997, 2809, (Csp^3-H), 1670 (**CO**NH), 1428, 1342 (Csp^3-H bending): ^{1}H-NMR ($CDCL_3$, 300MHz): δ 7.65 (s, 1H, N-H), 7.58-7.21 (m, 9H, Ar-H), 3.12 (s, 3H), 2.53 (s, 3H), 2.37 (s, 3H); ^{13}C-NMR ($CDCL_3$, 75MHz): δ 168.63 (**CO**NH), 161.50 (-C=C-**CO**-N-), 149.05, 136.81, 134.54,131.24, 131.00, 130.80, 130.41, 129.28, 124.21,36.27 (**CH$_3$**-N-), 20.16 (**CH$_3$**-C_{SP}^2-), 12.78 (**CH$_3$**-Ar-C). GC-MS (m/z): 321 M^+, 245, 187, 119 (100%), 91, 56. Elemental analysis found $C_{19}H_{19}N_3O_2$: C 72.32, H 5.25, N 13.05.

***N*-(1,5-Dimethyl-3-oxo-2-phenyl-2,3-dihydro-1*H*-pryazole-4-yl)-4-methylbenzamide (4c):**

Yellow crystalline solid; Yield; 85%, m.p: 183-184 °C; IR (neat): 3145 (CO**NH**), 2954, 2891, (Csp^3-H), 1637 (**CO**NH), 1425, 1347 (Csp^3-H bending): ^{1}H-NMR ($CDCL_3$, 300MHz): δ 8.04 (s, 1H, N-H), 7.78 (d, 2H, Ar-H, *J* = 6Hz), 7.47-7.40 (m, 4H, Ar-H), 7.33-7.21 (m, 3H, Ar-H), 3.10 (s, 3H), 2.39 (s, 3H), 2.32 (s, 3H); ^{13}C-NMR ($CDCL_3$, 75MHz): δ 166.09 (**CO**NH), 161.86 (-C=C-**CO**-N-), 149.31, 142.27, 134.66, 130.87, 129.27, 129.19, 127.50, 126.98, 124.33, 109.07, 36.23 (**CH$_3$**-N-), 21.49 (**CH$_3$**-C_{SP}^2-), 12.68 (**CH$_3$**-Ar-C).LC-MS (m/z) %: M^+322. Elemental analysis found $C_{19}H_{19}N_3O_2$: C 72.32, H 5.25, N 13.05.

2-Chloro-*N*-(1,5-dimethyl-3-oxo-2-phenyl-2,3-dihydro-1*H*-pryazole-4-yl)benzamide (4d):

Yellow crystalline solid; Yield; 82%, m.p: 103-104 °C; IR (neat): 3150 (CO**NH**), 2991, 2865, (Csp^3-H), 1675 (**CO**NH), 1435, 1346 (Csp^3-H bending): ^{1}H-NMR ($CDCL_3$, 300MHz): δ 7.64-7.60 (m, 3H, Ar-H), 7.45 (m, 2H, Ar-H), 7.40 (m, 3H, Ar-H), 7.37-7.26 (m, 2H, Ar-H, s, 1H, N-H), 3.13 (s, 3H), 2.41 (s, 3H); ^{13}C-NMR ($CDCL_3$, 75MHz): δ 166.25 (**CO**NH), 161.36 (-C=C-**CO**-N-), 149.45, 137.40, 134.55,133.40, 131.45, 129.63, 129.24, 127.48, 126.98, 124.21, 119.70, 108.31, 36.17 (**CH$_3$**-N-), 12.79 (**CH$_3$**-C_{SP}^2-H). LC-MS (m/z) %: M^+342 (1:3), 214. Elemental analysis found $C_{18}H_{16}ClN_3O_2$: C 61.25, H 6.72, N 14.42.

4-Chloro-*N*-(1,5-dimethyl-3-oxo-2-phenyl-2,3-dihydro-1*H*-pryazole-4-yl)benzamide (4e):

Yellow crystalline solid; Yield; 86%, m.p: 113-114°C; IR (neat): 3151 (CO**NH**), 2993, 2876, (Csp^3-H), 1674 (**CO**NH), 1425, 1341 (Csp^3-H bending): ^{1}H-NMR ($CDCL_3$, 300MHz): δ 7.97-7.94 (m, 2H, Ar-H), 7.55-7.41 (m, 7H, Ar-H, s, 1H, N-H), 3.31 (s, 3H), 2.26 (s, 3H); ^{13}C-NMR

($CDCL_3$, 75MHz): δ 164.66 (**CO**NH), 161.86 (-C=C-**CO**-N-), 152.91, 136.44, 135.04, 132.49, 129.56, 129.07, 128.44, 126.24, 123.51, 35.94 (**CH_3**-N-), 10.97 (**CH_3**-C_{SP}^2-).LC-MS (m/z) %: M^+342 (1:3), 278, 214. Elemental analysis found $C_{18}H_{16}ClN_3O_2$: C 61.25, H 6.72 , N 14.42.

2-Bromo-*N*-(1,5-dimethyl-3-oxo-2-phenyl-2,3-dihydro-1*H*-pryazole-4-yl)benzamide (4f):

Brown crystals, Yield; 87%, m.p: 108-109 °C ; IR (neat): 3151 (CO**NH**), 2990, 2832, (Csp^3-H), 1678 (**CO**NH), 1423, 1332 (Csp^3-H bending): ^{1}H-NMR ($CDCL_3$, 300MHz): δ 7.81 (s, 1H, N-H), 7.66-7.28 (m, 9H, Ar-H), 3.15 (s, 3H), 2.48 (s, 3H) ; ^{13}C-NMR ($CDCL_3$, 75MHz): δ 166.31 (**CO**NH), 161.19 (-C=C-**CO**-N-), 36.09 (**CH_3**-N-), 12.81 (**CH_3**-C_{SP}^2-), 149.37, 137.29, 134.37 ,133.46, 131.56, 129.63, 129.33, 127.56, 124.40. GC-MS (m/z): 387 (M^+), 341, 321 (100%), 202, 119, 91, 56.LC-MS (m/z) %: M^+386 (1:1), 368, 214, 203. Elemental analysis found $C_{18}H_{16}BrN_3O_2$: C 59.47, H 4.06, N 9.19.

***N*-(1,5-Dimethyl-3-oxo-2-phenyl-2,3-dihydro-1*H*-pryazole-4-yl)-3,5-dihydroxybenzamide (4g):**

Brownish black amorphous solid; Yield; 82%, m.p: 163-164 °C; IR (neat): 3159 (CO**NH**), 2927, 2815, (Csp^3-H), 1679 (**CO**NH), 1422, 1332 (Csp^3-H bending): ^{1}H-NMR ($CDCL_3$, 300MHz): δ 8.79 (s, 1H, N-H), 7.21 (m, 2H, Ar-H), 6.92 (m, 3H, Ar-H), 6.58 (m, 2H, Ar-H), 3.27 (s, 3H), 2.37 (s, 3H); ^{13}C-NMR ($CDCL_3$, 75MHz): δ 165.62 (**CO**NH), 162.53 (-C=C-**CO**-N-), 158.73. 158.28, 144.74, 142.74, 129.32, 129.08, 126.04, 124.67, 123.41, 123.27, 108.12, 106.36, 36.12(**CH_3**-N-), 11.03 (**CH_3**-C_{SP}^2-).LC-MS (m/z) %: M^+340, 322, 214, 135. Elemental analysis found $C_{18}H_{17}N_3O_4$: C 62.00, H 6.76, N 11.01.

***N*-(1,5-Dimethyl-3-oxo-2-phenyl-2,3-dihydro-1*H*-pryazole-4-yl)-4-phenylbutanamide (4h):**

Yellow solid; Yield; 84%, m.p: 137-138 °C; IR (neat): 3256 (CO**NH**), 2923, 2827, (Csp^3-H), 1659 (**CO**NH), 1433, 1352 (Csp^3-H bending): ^{1}H-NMR ($CDCL_3$, 300MHz): δ 8.80 (d, 2H, Ar-H), 8.37 (d, 1H, Ar-H), 8.20 (s, 1H, N-H), 3.55 (2H, t, 9Hz),1.81 (m, 2H),3.08 (s, 3H); ^{13}C-NMR ($CDCL_3$, 75MHz): δ 177.30 (**CO**NH), 173.29 (-C=C-**CO**-N-), 161.08, 149.27, 144.94, 141.78, 140.25, 134.07, 128.54, 128.47, 127.44, 126.83, 123.26, 54.22 (-CO-C**H_2**-C-), 35.83 (**CH_3**-N-), 26.56(**CH_3**-C_{SP}^2-), 12.32 (-CH_2-C**H_2**-Ar-), 12.20 (-CH_2-C**H_2**-CH_2-).LC-MS (m/z) %: M^+349, 348, 232, 214.Elemental analysis found $C_{21}H_{23}N_3O_2$: C 70.18, H 8.83, N 10.00.

***N*-(1,5-Dimethyl-3-oxo-2-phenyl-2,3-dihydro-1*H*-pryazole-4-yl)furan-2-carboxamide (4i):**

Red crystalline solid, Yield; 83%, m.p: 143-144 °C; IR (neat): 3146 (CO**NH**), 2953, 2896, (Csp^3-H), 1634 (**CO**NH), 1455, 1327 (Csp^3-H bending): ^{1}H-NMR ($CDCL_3$, 300MHz): δ 8.52 (s, 1H, N-H), 7.60-7.52 (m, 4H, Ar-H), 7.41-7.36 (m, 3H, Ar-H,), 6.49 (d, 1H, C-4-Furoic ring, *J* = 1.8Hz), 6.49 (s, 1H), 3.42 (s, 3H), 2.96 (s, 3H) ; ^{13}C-NMR ($CDCL_3$, 75MHz): δ 161.91 (**CO**NH), 156.27 (-C=C-**CO**-N-), 155.55, 148.70, 145.83, 132.26, 130.10, 130.01, 116.97, 112.29,107.56, 33.60 (**CH_3**-N-), 14.80 (**CH_3**-C_{SP}^2-). GC-MS (m/z): 387 (M^+), 341, 321 (100%), 202, 119, 91, 56. LC-MS (m/z) %: M^+322, 233, 215, 214. Elemental analysis found $C_{16}H_{15}N_3O_3$: C 63.56, H 5.12, N 15.08.

***N*-(1,5-Dimethyl-3-oxo-2-phenyl-2,3-dihydro-1*H*-pryazole-4-yl)pivalamide (4j):**

Yellow amorphous solid, Yield; 86%, m.p: 127-128 °C ; IR (neat): 3250 (CO**NH**), 2978, 2932, (Csp^3-H), 1644 (**CO**NH), 1456, 1337 (Csp^3-H bending): ^{1}H-NMR ($CDCL_3$, 300MHz): δ 7.45-7.28 (m, 4H, Ar-H), 7.26 (m, 1H, Ar-H), 7.07 (s, 1H), 3.05 (s, 3H), 2.26 (s, 3H), 1.31 (s, 9H, CH_3) ; ^{13}C-NMR ($CDCL_3$, 75MHz): δ 177.47 (**CO**NH), 161.68 (-C=C-**CO**-N-), 148.92, 134.81, 129.17, 126.66, 123.80, 39.28 (**CH_3**-N-), 36.49 (**CH_3**-C_{SP}^2-H), 27.67 (-CO-C-**C**H_3). GC-MS (m/z): 387 (M^+), 341, 321 (100%), 202, 119, 91, 56.LC-MS (m/z) %: M^+288, 214, 135. Elemental analysis found $C_{16}H_{21}N_3O_2$: C65.82, H7.43, N 14.67.

Biochemical Assays

Cell Transfection with Human APs and e5-NT

The COS-7 cells were transfected with plasmids expressing human APs: TNAP, IAP, PLAP & GCAP [19] or ecto-5'-nucleotidase either human or rat[5] in 10-cm plates, by using Lipofectamine. The confluent cells were incubated for 5 h at 37 °C in DMEM/F-12 in the absence of fetal bovine serum and with 6 µg of plasmid DNA and 24 µL of Lipofectamine reagent. The same volume of DMEM/F-12 containing 20% FBS was added to stop the transfection and cells were harvested 48–72 h later.

Preparation of membrane fractions

These transfected cells were washed three times with Tris–saline buffer at 4 °C and then the cells were collected by scraping in the harvesting buffer (95 mM NaCl, 0.1 mM PMSF, and 45 mM

Tris buffer, pH 7.5). The cells were washed twice by centrifugation at 300×*g* for 5 min at 4 °C.[5] Later the cells were resuspended in the harvesting buffer containing 10 µg/mL aprotinin and then sonicated. Cellular and nuclear debris were discarded by 10 min centrifugation (300×*g* at 4 °C). Glycerol (final concentration of 7.5%) was added to the resulting supernatant and all the samples were kept at -80 °C until used. Bradford microplate assay[20] was used for the estimation of protein concentration. Bovine serum albumin was used as a reference standard.

Protocol of Alkaline Phosphatase Assay (*h*-TNAP, *h*-IAP, *h*-PLAP and *h*-GCAP)

The determination of phosphatase activity with *h*-TNAP, *h*-IAP, *h*-PLAP and *h*-GCAP in presence or absence of the tested compounds, was performed with a chemiluminescent substrate, CDP-star. The conditions for the assay were optimized with the slight modifications in previously used spectrophotometric method.[3] The composition of assay buffer was: 2.5 mM $MgCl_2$, 0.05 mM $ZnCl_2$ and 8 M DEA (pH 9.8). Initial screening of the tested compounds was performed at a concentration of 0.2 mM. The total volume of 50 µL contained 10 µL of tested compound (0.2 mM with final DMSO 1% (v/v)), 20 µL of *h*-TNAP (46 ng of protein from COS cell lysate in assay buffer) or of *h*-IAP (57 ng protein in assay buffer) or of *h*-PLAP (55 ng protein in assay buffer) or of *h*-GCAP (51 ng protein in assay buffer), depending on assay. The mixture was pre-incubated for 5 to 7 minutes at 37 ^{o}C and luminescence was measured as pre-read using microplate reader (BioTek FLx800, Instruments, Inc. USA). Then, 20 µL of CDP-star (final concentration of 110 µM) was added to initiate the reaction and the assay mixture was allowed to incubate for 15 min more at 37 ^{o}C. The change in the luminescence was measured as after-read. The activity of each compound was compared with total activity control (without any inhibitor). Levamisole (2 mM per well) and L-phenylalanine (4 mM per well) were used as a positive control for the inhibition of *h*-TNAP and *h*-IAP, respectively. For the compounds which exhibited over 50% inhibition of either enzyme activity, full concentration inhibition curves were produced to evaluate IC_{50} values. All experiments were performed in triplicate. The IC_{50} values were calculated by using using a non-linear curve fitting program PRISM 5.0 (GraphPad, San Diego, California, USA).

Ecto-5′-nucleotidase Inhibition Assay

At the beginning of each day, the capillary was conditioned with the following sequence to obtain the highly reproducible migration times and good separation peaks: (i) rinse with 0.1 N NaOH for 5 min (ii) rinse with distilled water for 5 min and (iii) rinse with running buffer (sodium tetra borate 20 mM, pH 9.0) for 5 min.

The bioactivity assay of both rat and human Ecto-5′-nucleotidase was performed with the slight modifications in the method as described previously.[21] Stock solutions of 10 mM concentration of each compound were prepared in DMSO. Working solutions were prepared by appropriately diluting the stock solutions to 1 mM concentration in assay buffer (2 mM $MgCl_2$, 1 mM $CaCl_2$ and 10 mM Tris HCl, pH 7.4). The volume of the final assay was kept 100 µL. A 10 µL of each tested compound was pre-incubated with 10 µL of human e5NT (6.94 µg/mL) protein extract or rat e5NT (7.17 µg/mL) for 10 min in the presence of 70 µL assay buffer (2 mM $MgCl_2$, 1 mM $CaCl_2$ and 10 mM Tris HCl, pH 7.4). Afterwards, 10 µL of AMP substrate (final concentration of 500 µM) was added to initiate the enzymatic reaction. The reaction mixture was allowed to incubate for 10 min at 37 ^{o}C. To stop the enzymatic reaction, the reaction mixture was quenched by thermal denaturation at 99 ^{o}C for 20 min. Aliquots of 50 µL of each reaction mixture were transferred to CE minivial and injected into the CE instrument for data collection and analysis. Prior to each injection, the capillary was rinsed with 0.1 N NaOH for 2 min, distilled water for 2 min, and running buffer (sodium tetra borate 20 mM, pH 9.00) for 2 min. The enzyme reaction mixture was hydrodynamically injected into the capillary by applying pressure of 0.5 psi for 5s, followed by the application of 15 kV voltage for separation of peaks of substrate and product. The concentration of product i.e. Adenosine was determined by calculating the area under its absorbance peak at 260 nm. The compounds which exhibited over 50% inhibition of either the *r*-e5NT or *h*-e5NT activity were further evaluated for determination of IC_{50} values. For this purpose serial dilutions of each compound were prepared in assay buffer and their dose response curves were obtained by assaying each inhibitor concentration against both nucleotidases using the above mentioned reaction conditions. All experiments were performed in triplicate. The IC_{50} values were calculated by using a non-linear curve fitting program PRISM 5.0 (GraphPad, San Diego, California, USA).

Kinetics Study (Alkaline Phosphatase)

The inhibitors (compounds) with potent IC_{50} values were then selected for the kinetics study in order to determine their type of inhibition. Changes in the initial velocities of the reaction were measured at different concentrations of the inhibitor (0 μM, 0.5 μM, 1.00 μM, 2.00 μM) using substrate (CDP-star) concentrations of 55μM, 110 μM, 165 μM & 220 μM. A double-reciprocal plot of the inhibition kinetics of h-TNAP by **4i** & **4h** by h-IAP and **4f** by h-PLAP by inhibitor was measured by using PRISM 5.0 (GraphPad, San Diego, California, USA).

4i (TNAP)

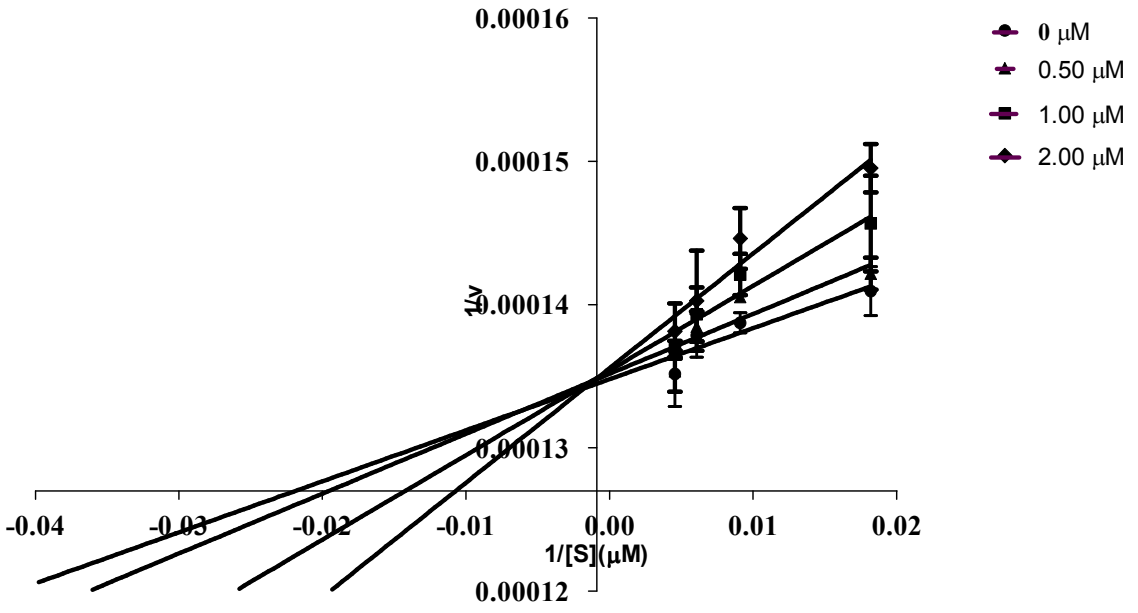

Figure 1. Double-reciprocal plots of the inhibition kinetics of bovine tissue non-specific alkaline phosphatase (TNAP) indicating competitive inhibition by compound **4i**. Changes in the initial velocities of the reaction were measured at different concentrations of the inhibitor **4i** using substrate CDP-Star (disodium 2-chloro-5-(4-methoxyspiro[1,2-dioxetane-3,2′-(5-chlorotricyclo[3.3.1.13.7]decan])-4-yl]-1-phenyl phosphate).

4h (IAP)

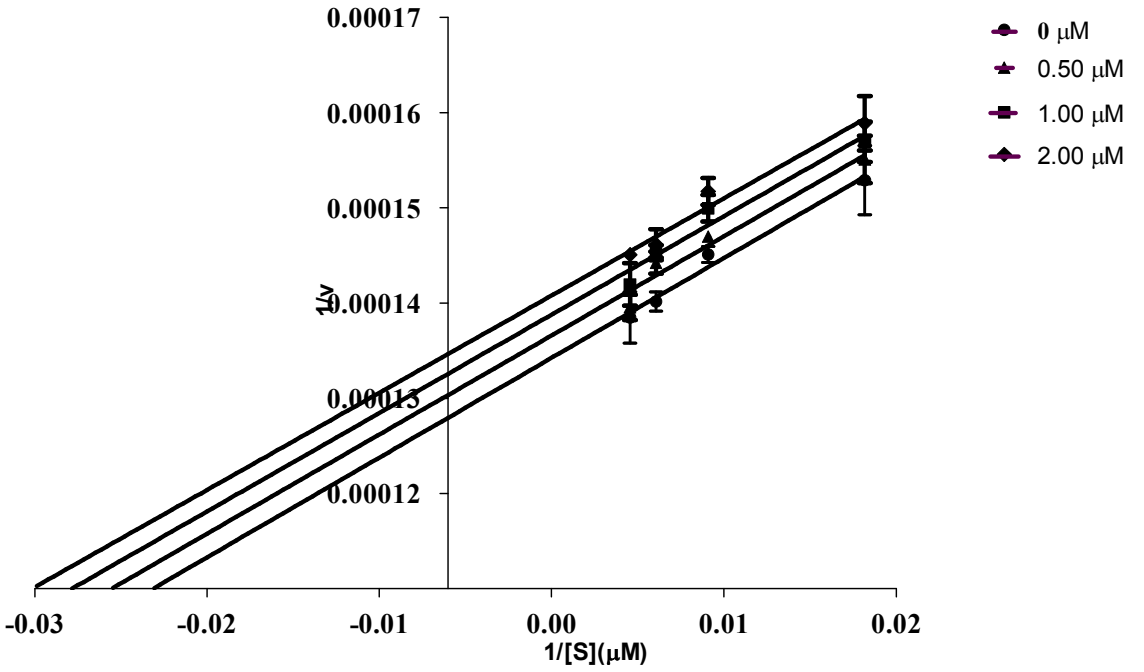

Figure 2. Double-reciprocal plots of the inhibition kinetics of tissue specific alkaline phosphatase (IAP) indicating competitive inhibition by compound **4h**. Changes in the initial velocities of the reaction were measured at different concentrations of the inhibitor **4h** using substrate CDP-Star (disodium 2-chloro-5-(4-methoxyspiro[1,2-dioxetane-3,2′-(5-chlorotricyclo[3.3.1.13.7]decan])-4-yl]-1-phenyl phosphate).

4f (h-PLAP)

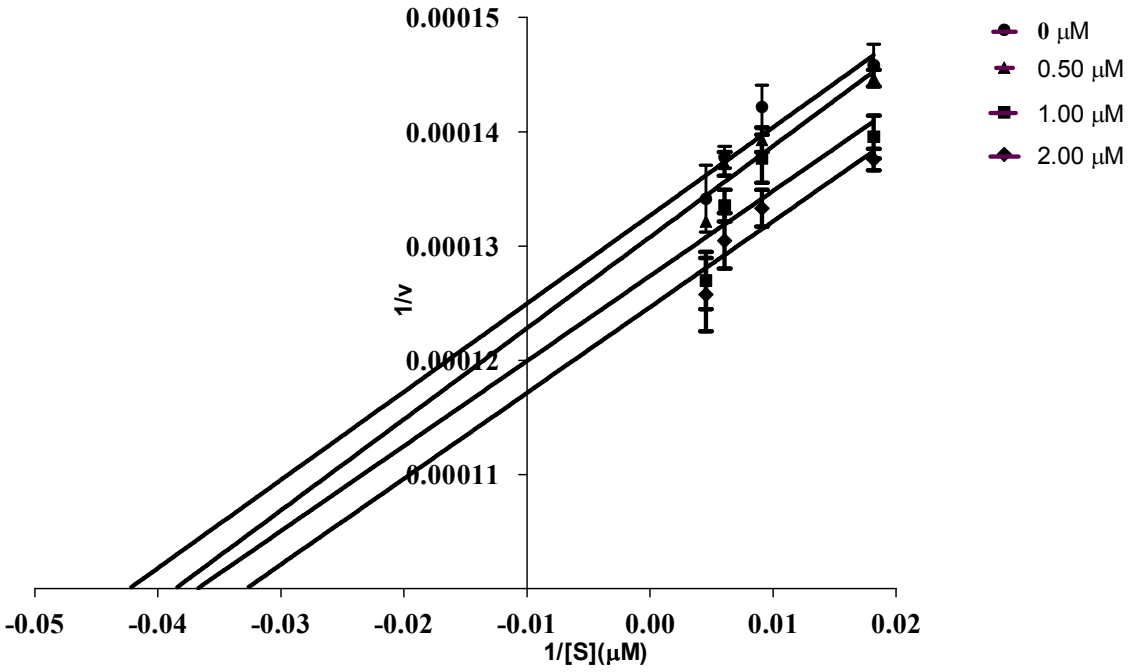

Figure 3. Double-reciprocal plots of the inhibition kinetics of tissue specific alkaline phosphatase (h-PlAP) indicating competitive inhibition by compound **4f**. Changes in the initial velocities of the reaction were measured at different concentrations of the inhibitor **4f** using substrate CDP-Star (disodium 2-chloro-5-(4-methoxyspiro[1,2-dioxetane-3,2′-(5-chlorotricyclo[3.3.1.13.7]decan])-4-yl]-1-phenyl phosphate).

Homology modelling of Human Alkaline Phosphatases (*h-TNAP*, *h*-IAP, *h*-GCAP)

Since crystal structures of human tissue non-specific alkaline phosphatase (*h*-TNAP), intestinal alkaline phosphatase (*h*-IAP) and germ-cell alkaline phosphatase (*h*-GCAP) have not yet been determined experimentally, therefore homology models of *h*-TNAP, *h*-IAP and *h*-GCAP were generated using Chimera[22] and Modeller.[23] Sequences of all three human AP enzymes, *h*-TNAP (uniprot id: P05186), *h*-IAP (uniprot id: P09923), and *h*-GCAP (uniprot id: P10696) were fetched in Chimera. A search on BLAST database[24] returned *h*-PLAP (PDB id: 1ZED; uniprot id: P05187) among top five searched results for all APs, therefore *h*-PLAP was selected to be used as a template protein. The sequences of target proteins were added to that of template

protein via Needleman Wunsch global alignment algorithm[25] embedded in Chimera. The structures of all target proteins *h*-TNAP, *h*-IAP and *h*-GCAP were modelled using Modelle[23]. Ramachandran plots were generated using Molprobity[26]. Comparative sequence alignments and Ramachandran plots are given in supporting information, Figures S6-S8 and Figures S2-S4, respectively. All active site residues among modelled proteins (*h*-TNAP, *h*-IAP, *h*-GCAP), and *h*-PLAP were found to be highly conserved (Table 1). Amino acid residues Phe107, Gln108, Ser155 and Glu429 in *h*-PLAP have been replaced by amino acid residues Glu108, Gly109, Thr156 and His434 respectively in *h*-TNAP. Glu429 of *h*-PLAP, was found to be the only active site amino acid residue that was not conserved in any of the *h*-APs, in *h*-IAP it is replaced by a Ser448 residue, whereas in *h*-GCAP, it has been replaced by Gly448 residue. Figures 1-3 show comparison of active site residues of modelled proteins *h*-TNAP, *h*-IAP and *h*-GCAP against the template protein *h*-PLAP.

Homology modelling of Rat ecto-5′-Nucleotidase (*r*-e5NT)

Crystal structure of rat ecto-5′-nucleotidase (*r*-e5NT), is not available from the Protein Data Bank (PDB), therefore its homology model was generated using Chimera[22] and Modeller[23]. The protein sequence of *r*-e5NT (uniprot id: Q66HL0) was fetched in Chimera. A search on BLAST database[24] indicated human ecto-5′-nucleotidase (*h*-e5NT), (PDB id: 4H2I; uniprot id: P21589) among top five results (sharing 88% sequence identity), and was therefore selected to be used as a template protein for modelling of *r*-e5NT. The sequences of target protein (*r*-e5NT) was added to that of template protein (*h*-e5NT) via Needleman Wunsch global alignment algorithm[25] embedded in Chimera. The structure of target protein, *r*-e5NT, was modelled using Modeller[23] Ramachandran plots were generated using Molprobity[26]. Five models were generated, each model was analyzed individually and the most favorable model, having 87.97% identity and 0.141 rmsd was selected. Comparative sequence alignment and Ramachandran plot are given in supporting information, Figures S1 and Figures S5, respectively. Active site residues among modelled proteins (*r*-e5NT), and target protein (*h*-5T) were found to be highly conserved. Comparison of active site residues of *r*-e5NT and *h*-e5NT are given in Figure 4.

Molecular Docking

In order to rationalize most plausible binding site interactions of inhibitors, molecular docking studies were carried out against three homology built models of alkaline phosphatases (*h*-TNAP, *h*-IAP and *h*-GCAP), and one experimentally determined *h*-PLAP (PDB id: 1ZED). Crystal structure of closed (active) form human ecto-5′-nucleotidase (*h*-e5NT) in complex with inhibitor adenosine 5′-(α,β-methylene)diphosphate (AMPCP) was downloaded from the Protein Data Bank (PDB id 4H2I).[27] Prior to docking the enzymes (receptors) were prepared for docking using DockPrep utility of Chimera, whereby all hetero and solvent molecules are removed, hydrogen atoms and Gasteiger chargers are added and incomplete side chains (if any) are repaired using Dunbrack Rotamer library. All alkaline phosphatases, contain two zinc ions and one magnesium ion intheir active sites, charges of +2 were assigned on each metallic center. Human ecto-5′-nucleotidase (*h*-e5NT) contains only two zinc ions in its active site, charge of +2 was assigned to each zinc ion. Structures of all ligands were sketched in ChemSketch,[28] the geometries of all ligands were optimized using semi-empirical PM3 method in ArgusLab 4.0.1.[29] Molecular docking studies were carried out using BiosolveIT's LeadIT software version 2.1.8.[30] Docked conformations were analyzed using LeadIT and Discovery Studio Visualizer 4.0.[31] For *h*-e5NT method validation was carried out by re-docking the ligand (AMPCP) extracted from the crystal structure of *h*-e5NT in complex with AMPCP (PDB id 4H2I), the docking method was successfully able to reproduce the experimentally observed bound conformation of AMPCP with an rmsd of 1.7 Å

Results and Discussion

General procedure for the synthesis of*N*-(2,3-dimethyl-5-oxo-1-phenyl-2,5-dihydro-1*H*-pyrazol-4-yl)benzamides (4a-j)

A calculated amount of suitably substituted aromatic acids **1a-j** (0.5 mmol) was set to reflux with thionyl chloride (0.03 mL, 0.5 mmol) for the fresh preparation of respective acid halides (**2a-j**). The acid chlorides (**2a-j**) were added to the solution of 4-aminophenazone **3** (0.1g, 0.5 mmol), dissolved in pyridine (0.03 mL, 0.5 mmol) and the reaction mixture was refluxed for 3 hours. The completion of the reaction was confirmed by TLC, the solids appeared were filtered off and recrystallized by aqueous ethanol to afford the purified products (**4a-j**).

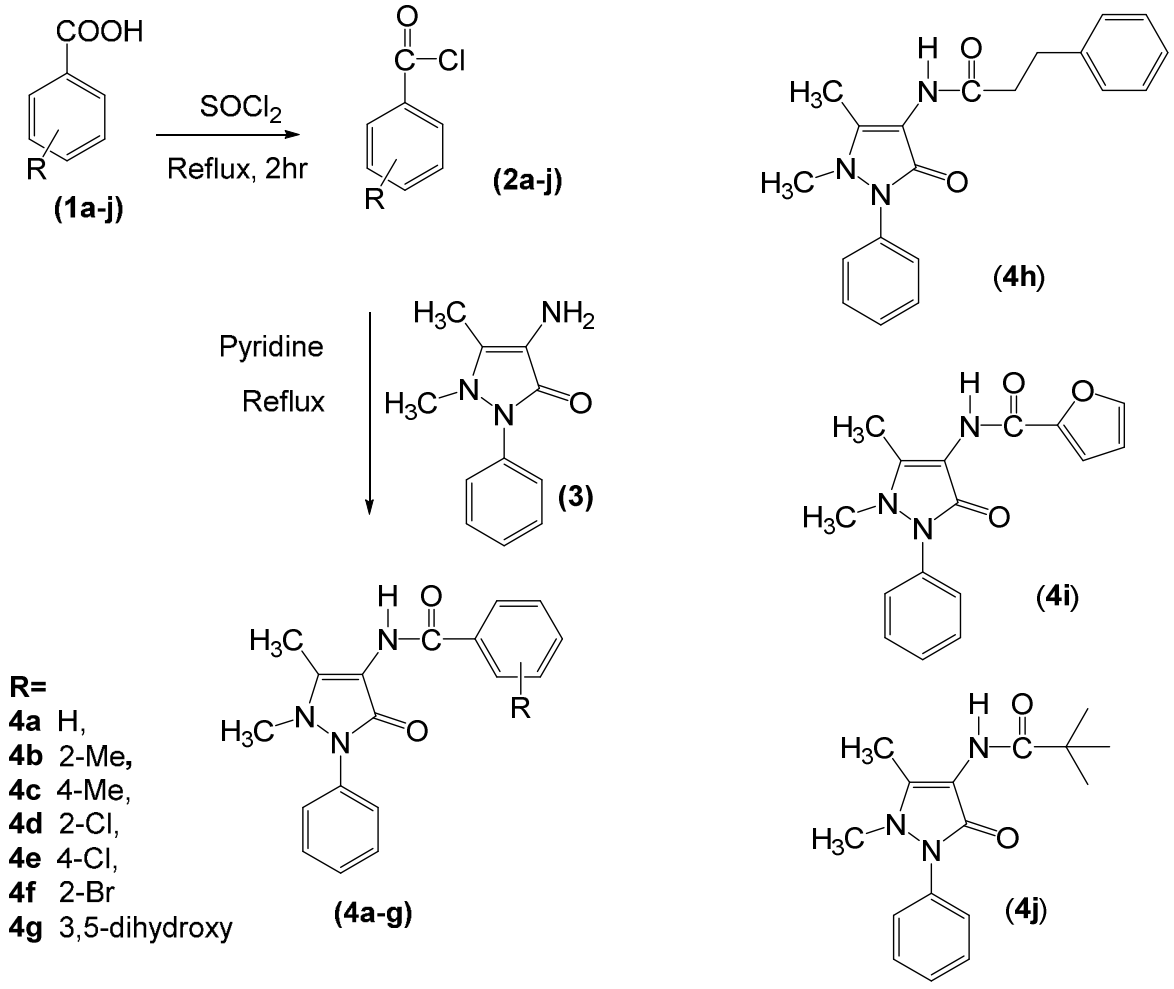

Scheme 1 Synthetic pathway to N-(2,3-dimethyl-5-oxo-1-phenyl-2,5-dihydro-1*H*-pyrazol-4-yl)benzamides **(4a-j)**

Chemistry

The synthetic pathway adopted for syntheses of title compounds is depicted in Scheme 1. The benzamides are easily accessible by reaction of suitably substituted acid chlorides to the solution of 4-aminophenazone in dry pyridine. The solids products obtained were recrystallized by aqueous ethanol to afford the purified products (**4a-j**). The spectral and microelemental data confirmed the structural assignments. The compound **4i** has already been reported.[32]

Alkaline Phosphatase and Ecto-5'-nucleotidase Activity and SAR:

Different benzamide derivatives of phenazone were synthesized and further evaluated for their anticancer properties. For this purpose in-vitro activity against membrane bounded nucleotidases including alkaline phosphatases and ecto-nucleotidase were performed. These compounds were found to inhibit all APs at the concentration of 200 μM. However, at the lower concentration of 100 μM these compounds significantly inhibited both human and rat e5-NT.

As regards to AP activity, the compounds were tested against four isozymes of human recombinant APs: *h*-TNAP, *h*-IAP, *h*-PLAP and *h*-GCAP. It was found that all the derivatives exhibited significant inhibitory potential against *h*-TNAP within the IC_{50} ± SEM values of 0.337±0.08 μM to 5.91±0.99 μM. Among ten derivatives, compound **4i** was the most potent inhibitor of *h*-TNAP with an IC_{50} value ±SEM of 0.337±0.08 μM which is 70 fold lower than the reference standard inhibitor Levamisole (IC_{50} ± SEM = 20.2 ± 1.9 μM). The detailed study of the structure showed that in this compound the benzene ring attached to acetamide group is replaced with the furan ring. Thus, the name benzamide is replaced with carboxamide. The hydrophilic character of the compound was increased as furan ring is electron donating and it increases the electron density of the compound by donating its lone pair of electrons to it, so increasing its hydrophilicity property. It can be suggested that the activity of this compound might be due to the presence of furan ring. Furthermore, this statement was proved by observing inhibitory values of the other compounds. The compounds having less carbon number are more active against *h*-TNAP than the compounds containing higher carbon number. The presence of halogens also affects the property of the compound. The compounds halogens are more lipophilic in character thus exhibiting lower IC_{50} values against *h*-TNAP as mentioned in the Table 1. On the other hand the inhibition of *h*-IAP by this compound increased with the hydrophobicity or lipophilicity character of the compound. In this case the maximum inhibition was shown by **4h** with an IC_{50} value of ± SEM = 2.83±0.03 μM which is 35 fold lower than the known reference standard inhibitor i.e. L-Phenylalanine (IC_{50} ± SEM = 100 ± 3 μM). With the decrease in lipophilic character other compounds inhibited more modestly as reported in Table 1.

When these compounds were tested for their inhibition potential against *h*-PLAP we observed that with the exception of compounds **4i** and **4j**, all the other derivatives were strong inhibitors of *h*-PLAP. In comparison to *h*-TNAP the inhibition of *h*-PLAP by these compounds was weaker but stronger than with reference inhibitor i.e Levamisole (IC_{50} ± SEM = 120.0 ± 2.51 μM). The

maximum inhibition was obtained in presence of compound **4c** and **4f** with IC_{50} value of 4.97±0.66 μM and 4.63±0.11 μM, respectively. Only few derivatives inhibited *h*-GCAP. The compound **4e** and **4g** inhibited this enzyme at a concentration of 180 and 300 fold less than the standard inhibitor L-Phenylalanine. The structures of these compounds showed that substitution at para position is important for inhibition of *h*-GCAP. However the presence of bulky groups and substitution at other sites will result in loss of *h*-GCAP inhibition by the compound.

When the benzamide derivatives were tested for inhibition of human and rat e5-NT it was observed that these compounds exhibited more inhibitory potential against e5-NT rather than the same member of the family i.e. APs (Table 1). The compounds **4c** and **4i** displayed strongest inhibition of *h*-e5-NT with IC_{50} value of 0.78±0.26 μM and 0.77±0.42 μM, respectively. The structures of these compounds showed electron donating groups i.e. methyl and furan respectively, which are responsible for their inhibitory behavior against human e5-NT. All derivatives inhibited rat e5-NT. The structure activity relationship of all derivatives displayed that the compound **4h** having substitution of large carbon chain showed the strongest inhibition of rat e5-NT with IC_{50} value 0.17±0.02 μM which is a concentration 450 fold lower than its previously mentioned standard inhibitor sulfamic acid. The compound **4g** was found to be the selective inhibitor of rat e5-NT with IC_{50} value 1.38±0.29 μM which is the concentration 55 fold lower than its previously mentioned standard inhibitor sulfamic acid. The reported compounds herein are of considerable interest for further applications in the field of medicinal chemistry as these compounds have potential to bind nucleotide protein targets.

Table 1. Alkaline phosphatase and Ecto-5-Nucleotidase inhibition in presence of the synthesized compounds

	Alkaline Phosphatase				Ecto-5'-nucleotidase	
Code	***h*-TNAP**	***h*-IAP**	***h*-PLAP**	***h*-GCAP**	***h*-e5-NT**	***r*-e5-NT**
	IC_{50} (μM) ±SEM	IC_{50} (μM) ±SEM	IC_{50} (μM) ±SEM	IC_{50} (μM) ±SEM	IC_{50} (μM) ±SEM	IC_{50} (μM) ±SEM
4a	4.22±0.34	12.3±1.08	8.58±0.91	4.94±0.23	1.49±0.86	23.5±0.87
4b	3.32±0.98	-	6.67±0.87	-	5.59±0.94	7.41±0.64
4c	5.91±0.99	3.27±0.67	4.97±0.66	7.63±0.99	0.78±0.26	0.83±0.41
4d	2.19±0.87	-	9.21±1.11	-	172.62±3.34	1.92±0.61
4e	0.691±0.11	-	10.5±1.09	1.65±0.22	1.25±0.38	1.05±0.46
4f	0.408±0.09	6.29±0.99	4.63±0.11	-	10.5±1.46	0.961±0.21
4g	5.15±1.01	15.1±1.06	10.9±1.22	1.03±0.11	-	1.38±0.29
4h	0.917±0.02	2.83±0.03	6.57±1 .02	-	17.9±1.87	0.174±0.02
4i	0.337±0.08	-	-	-	0.769±0.42	0.224±0.05
4j	4.36±0.71	-	-	-	7.36±0.41	0.625±0.18
Levamisole	19.2 ± 0.01	-	120.0 ± 2.51	-		
L-Phenylalanine	-	82.1 ± 0.01	-	301 ± 5.1		
Sulfamic acid					42.1±7.8	77.3±7.0

The IC_{50} is the concentration at which 50% of the enzyme activity is inhibited. Alkaline phosphatase (*h*-TNAP, *h*-IAP, *h*-PLAP and *h*-GAP) activity was performed at the final concentration of 200 μM. Ecto-5'-nucleotidase (human and rat) activity was done at final concentration of 100 μM.

Homology Modelling of *h*-TNAP, *h*-IAP and *h*-GCAP

Since crystal structures of humantissue non-specific alkaline phosphatase (*h*-TNAP), intestinal alkaline phosphatase (*h*-IAP) and germ-cell alkaline phosphatase (*h*-GCAP) are not available

from the Protein Data Bank (PDB), homology models of *h*-TNAP, *h*-IAP and *h*-GCAP were generated using Chimera[22] and Modeller.[23] The sequence of target proteins *h*-TNAP (uniprot id: P05186), *h*-IAP (uniprot id: P09923), and *h*-GCAP (uniprot id: P10696) were fetched in Chimera. BLAST (Basic Local Alignment Search Tool) protein database[24] was used to search for sequence similarity with target proteins, human placental alkaline phosphatase (*h*-PLAP, PDB id: 1ZED) was identified among the top five matches in all cases, and was accordingly selected to be used as a template. The sequence of template protein was added to the sequence of target protein using Needleman Wunsch global alignment algorithm[25] embedded in Chimera. Comparative modelling was run using Modeller via Chimera. The overall quality of the protein was evaluated, and Ramachandran plots were generated using Molprobity.[26] Comparative sequence alignments and Ramachandran plots are given in supporting information, Figures S6-S8 and Figures S2-S4, respectively. All active site residues among modelled proteins (hTNAP, hIALP, hGCALP), and hPALP were found to be highly conserved (Table 1). Amino acid residues Phe107, Gln108, Ser155 and Glu429 in hPALP have been replaced by amino acid residues Glu108, Gly109, Thr156 and His434 respectively in hTNALP. Glu429 of hPALP, was found to be the only active site amino acid residue that was not conserved in any of the hAPs, in hIALP it is replaced by a Ser448 residue, whereas in hGCALP, it has been replaced by Gly448 residue. Figures 1-3 show comparison of active site residues of modelled proteins hTNALP, hIALP and hGCALP against the template protein hPALP.

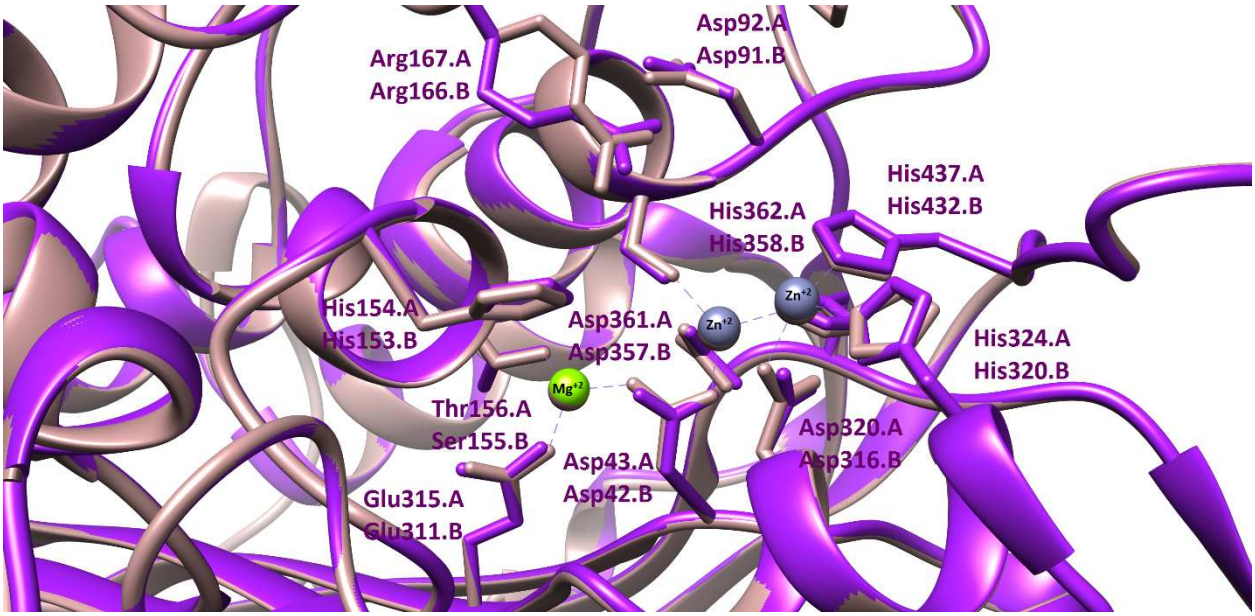

Figure 1. Comparison of active site residues of modelled *h*-TNAP (purple, A) with template *h*-PLAP (light brown, B).

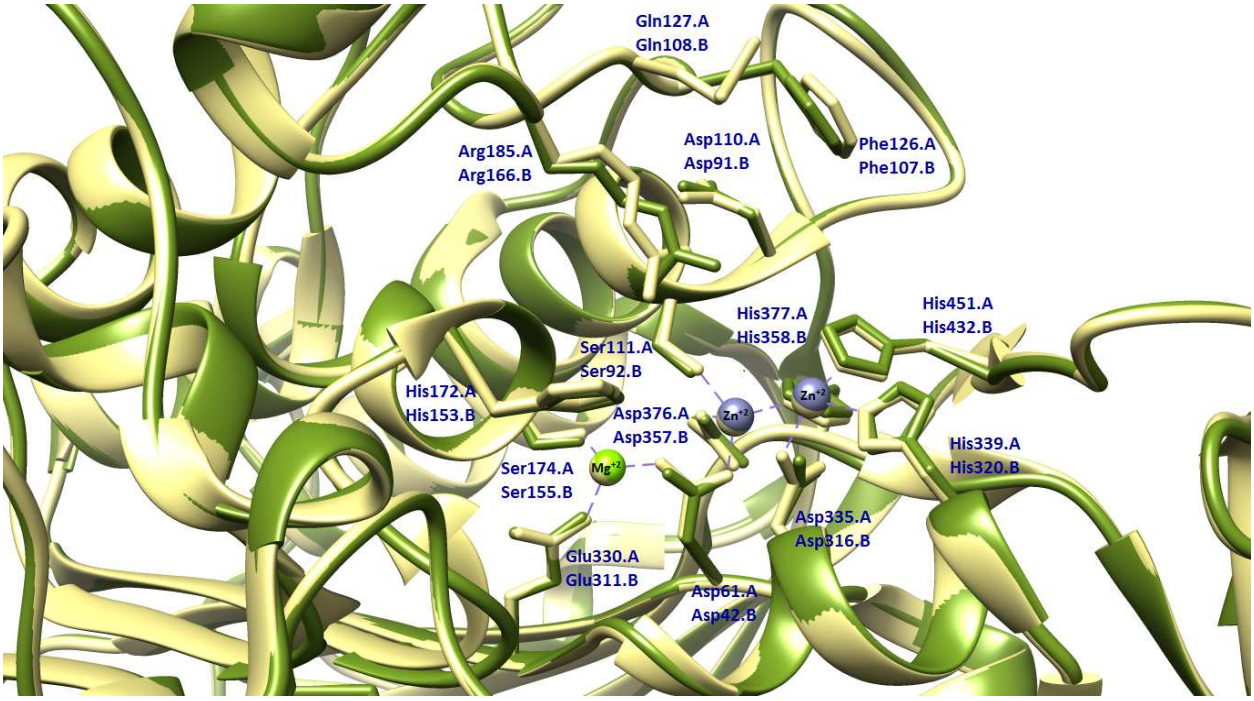

Figure 2. Comparison of active site residues of modelled *h*-IAP (green, A) with template *h*-PLAP (light brown, B).

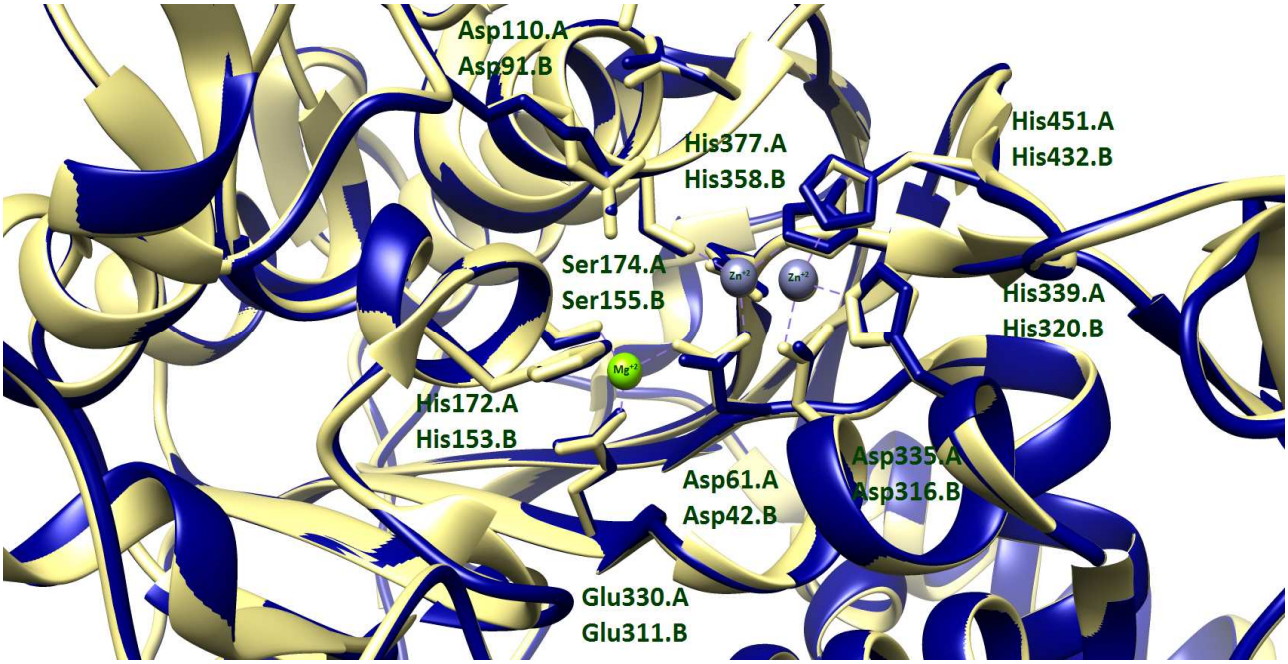

Figure 3. Comparison of active site residues of modelled *h*-GCAP (blue, A) with template *h*-PLAP (light brown, B).

Homology Modelling of Rat ecto-5′-Nucleotidase (*r*-e5NT)

Homology model of *r*-e5NT was generated using chimera[22] and Modeller.[23] The sequence of target protein *r*-e5NT (uniprot id: Q66HL0), was opened in Chimera. BLAST (Basic Local Alignment Search Tool) protein database[24] was used to search for sequence similarity with target proteins, human ecto-5′-nucleotidase (*h*-e5NT, PDB id: 4H2I) was identified among the top five matches, and was accordingly selected to be used as a template for modeling of *r*-e5NT. The sequence of template protein was added to the sequence of target protein using Needleman Wunsch global alignment algorithm[25] embedded in Chimera. Comparative modelling was run using Modeller.[23] The overall quality of the protein was evaluated, and Ramachandran plots were generated using Molprobity.[26]

Table 2. Comparison of active site residues of *h*-e5NT (PDB id: 4H2I) with *r*-e5NT. Conserved residues (with respect to *h*-e5NT) are in purple font color, the residues which are not conserved are in red font color.

***h*-e5NT**	***r*-e5NT**
Asp36	Asp38
His38	His40
Asp85	Asp87
Asn117	Asn119
His118	His120
His220	His222
His243	His245
Asn245	Asn247
Arg354	Arg356
Arg395	Arg397
Phe417	Phe419
Asp506	Asp508
Phe500	Tyr502

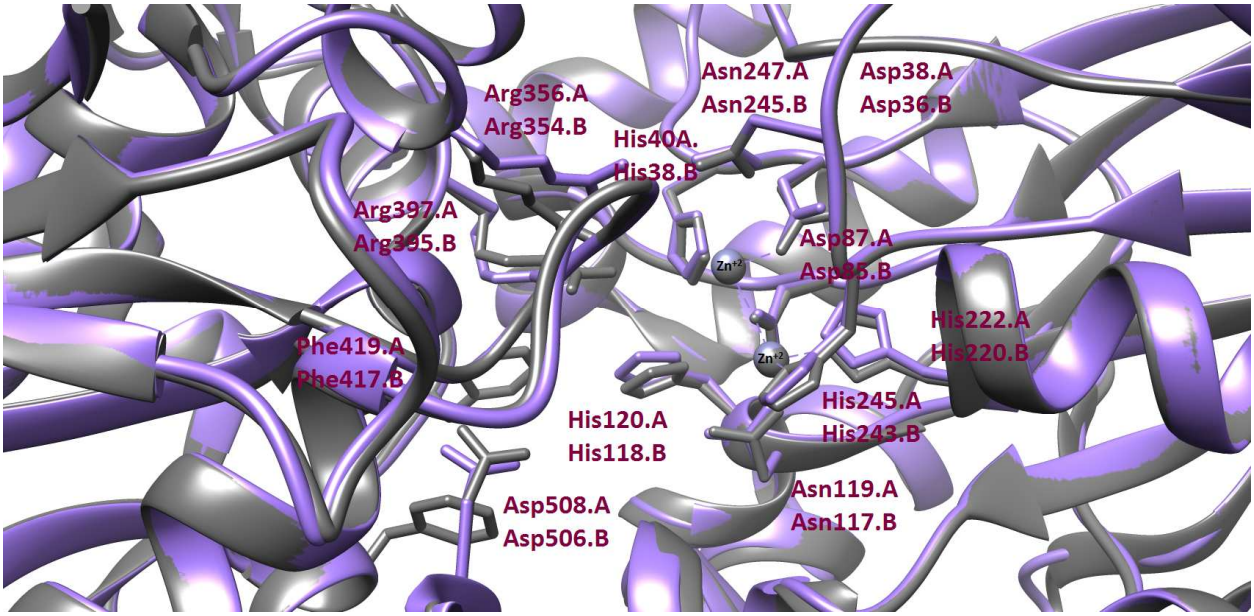

Figure 4. Comparison of active site residues of modelled *r*-e5NT (violet, A) with template *h*-e5NT (grey, B).

Molecular Docking

Molecular Docking Studies against ecto-5′-Nucleotidase (CD73)

Human ecto-5′-Nucleotidase (*h*-e5NT) Docking

Table 2 shows comparison of active site residues of human and rat e5NT, the differences in the amino acids that are not conserved, for example Phe500 in he5NT has been replaced by Tyr502 in re5NT, may contribute towards selectivity in inhibition exhibited by these compounds. Compound **4i** was found to be the most active *h*-e5NT inhibitor, and was therefore selected for molecular docking studies against *h*-e5NT (PDB id: 4H2I). No direct binding with the zinc ions was found. Detailed analysis of the docked mode of **4i** indicated presence of three hydrogen bonds, the oxygen atom of furan ring was found to act as a hydrogen bond acceptor towards amino group of Phe500 (2.34 Å). The amino group of amino acid Asn390 was making a bridging hydrogen bond with oxygen atom of carbonyl group of pyrazole ring (2.04 Å), and with oxygen atom of carboxamide group (2.14 Å). The 3D and 2D binding site interactions of **4i** are given in Figure 5.

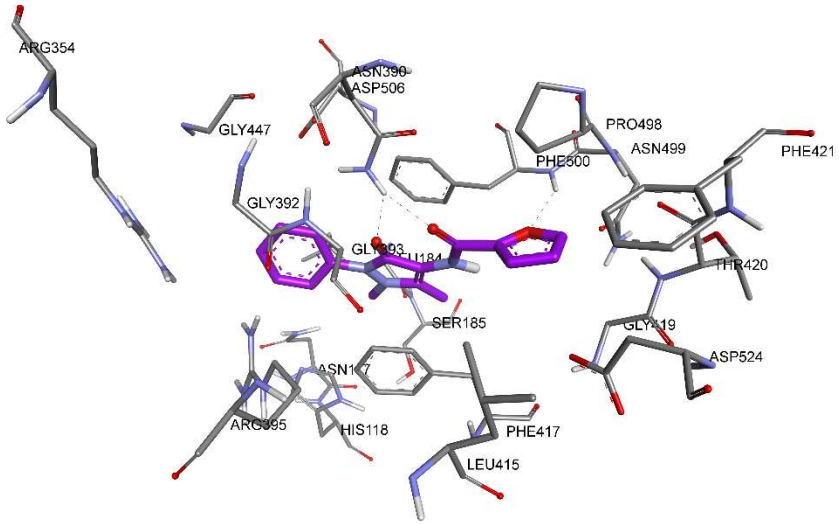

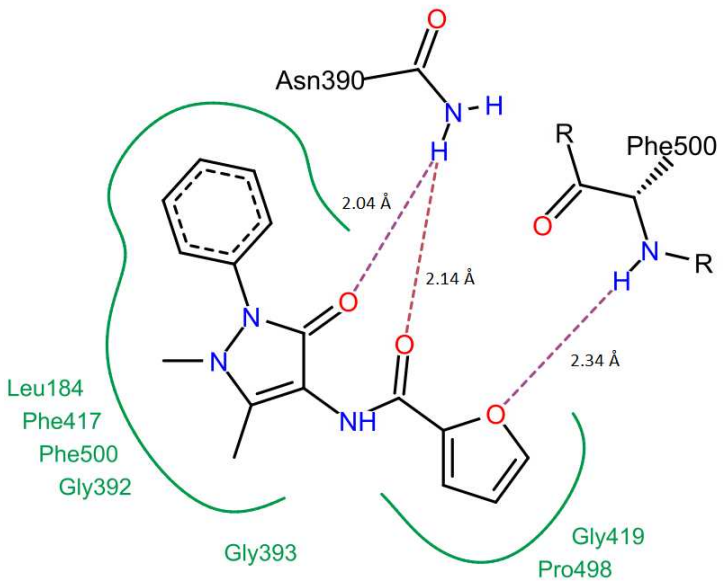

Figure 5. 3D and 2D binding site interactions of **4i** against *h*-e5NT.

Rat ecto-5′-Nucleotidase (*r*-e5NT) Docking

Compound **4h** was found to be the most active *r*-e5NT inhibitor, and was therefore selected for molecular docking studies against homology modelled *r*-e5NT. No direct binding with the zinc ions was found, the most hydrophobic part of the molecule, that is, ethylphenyl group was found to have a snug fit in the binding cavity of enzyme, surrounded by hydrophobic residues Phe419 and Leu186. The carboxamide group and the pyrazole ring were found to be surrounded by amino acid residues His120, Asn119 and His245. The NH of the carboxamide group was making a hydrogen bond with carbonyl oxygen atom of amino acid residue Leu186 (1.95 Å). The 3D and 2D binding site interactions of **4h** are given in Figure 6.

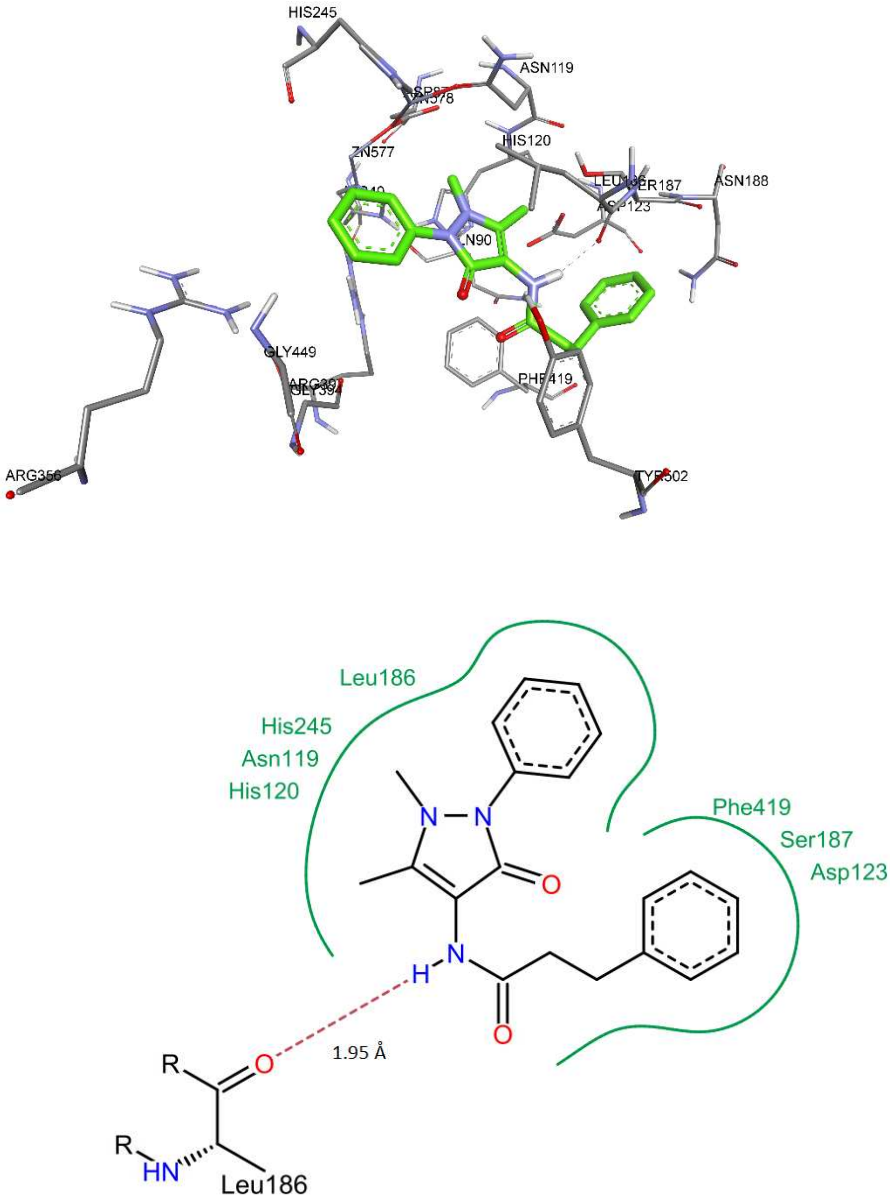

Figure 6. 3D and 2D binding site interactions of **4h** against homology modelled *r*-e5NT.

Molecular Docking Studies against Alkaline Phosphatases (APs)

Human Tissue Non-Specific Alkaline Phosphatase(*h*-TNAP) Docking

Detailed comparison of active site residues of different APs has been given in Table S1 of the supporting information, the differences in the amino acids that are not conserved may contribute towards selectivity in inhibition exhibited by these compounds. The most active *h*-TNAP

inhibitor **4i**, was subjected to molecular docking studies. Detailed analysis of binding site interactions reveal a directing binding of oxygen atom of furan ring with the catalytic zinc ion with a distance of 2.12 Å. The furan ring is surrounded by amino acid residues His321 and His324. The imidazole ring nitrogen atom the amino acid residue His437, was found to be involved in a hydrogen bond contact with the NH of carboxamide group of 4i at a distance of 2.08 Å. The NH group of same amino acid His437 was making another hydrogen bond (2.31 Å) with oxygen atom of carbonyl group of 4i. The 3D and 2D binding site interactions of **4i** are given in Figure 7.

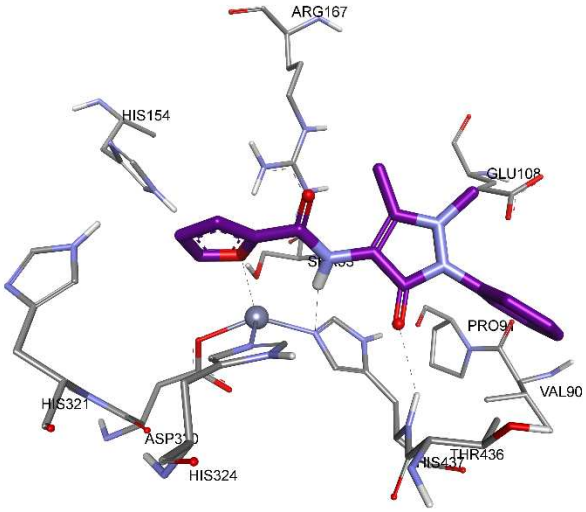

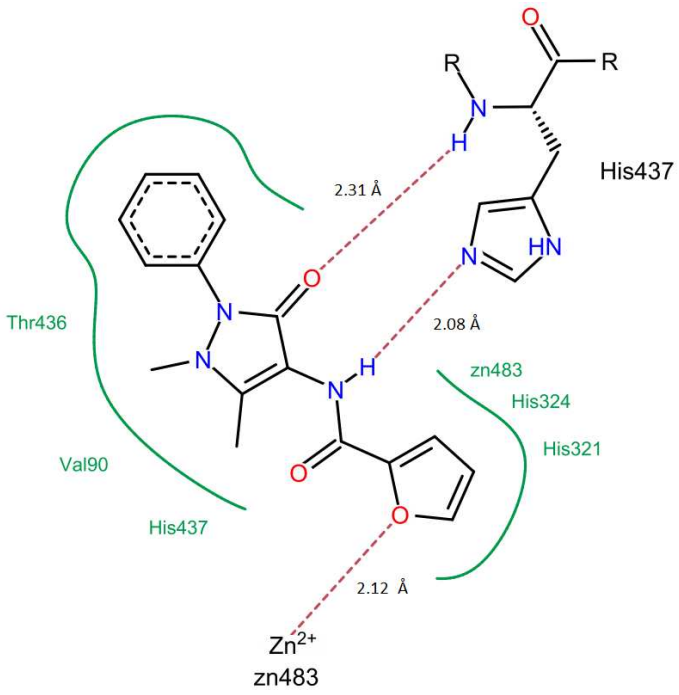

Figure 7. 3D and 2D binding site interactions of **4i.**

Human Intestinal Alkaline Phosphatase (*h*-IAP) Docking

The hydrophobic part, ethylphenyl, of the most active inhibitor **4h** was found to be surrounded by hydrophobic amino acid residues Phe126 and Val108, whereas the rest of the ligand was lying in close vicinity of the hydrophilic residues His339 and His336. The oxygen atom of the carboxamide group was making a hydrogen bond (2.12 Å) with NH group of His451 amino acid. A direct binding of carbonyl oxygen of pyrazole ring with the catalytic zinc ion was observed having a distance of 2.24 Å. Putative binding site interactions are given in figures below. The 3D and 2D binding site interactions of **4h** are given in Figure 8.

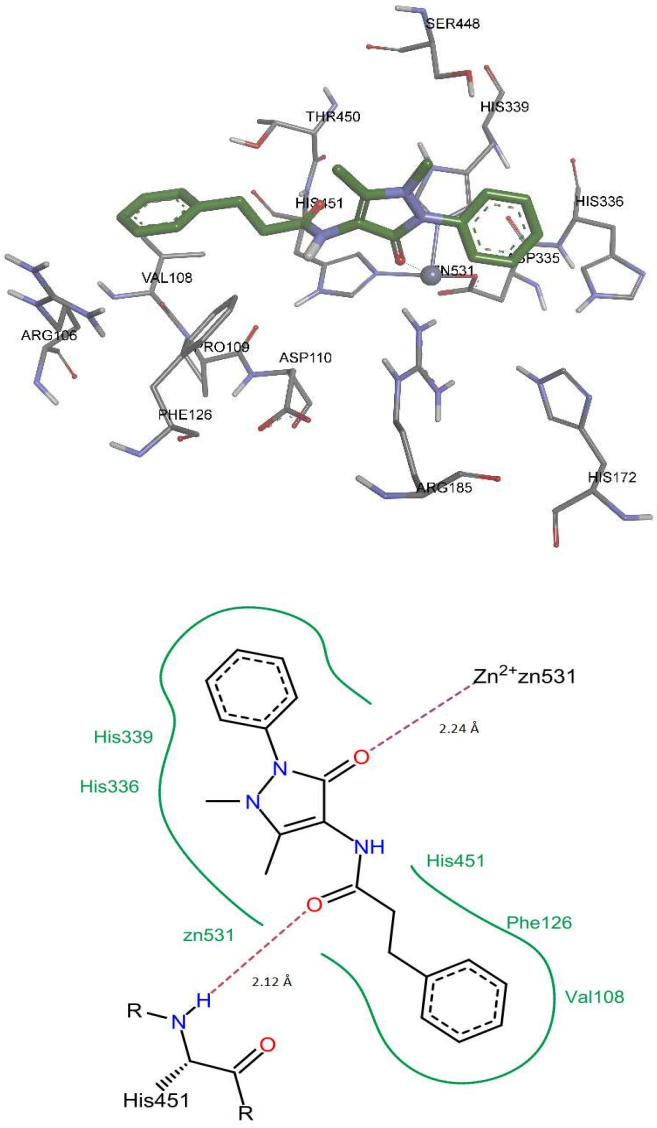

Figure 8. 3D and 2D binding site interactions of **4h.**

Human Germ Cell Alkaline Phosphatase (*h*-GCAP) Docking

Detailed molecular docking studies for compound **4g**, the most active *h*-GCAP were carried out using the homology modelled structure of *h*-GCAP. The docking studies revealed putative binding site interactions, which are given in figures below. Compound 4g was found to bind near the active site such that the phenyl pyrazole moiety was surrounded by amino acids Phe126, Thr450, Val108, His339 and His451. NH of carboxamide group was making a hydrogen bond with His451 at a distance of 2.21 Å.One of the hydroxyl substituent on the phenyl group was

making bridging hydrogen bonds with His172 (2.07 Å) and Asp335 (2.39 Å). The 3D and 2D binding site interactions of **4i** are given in Figure 9.

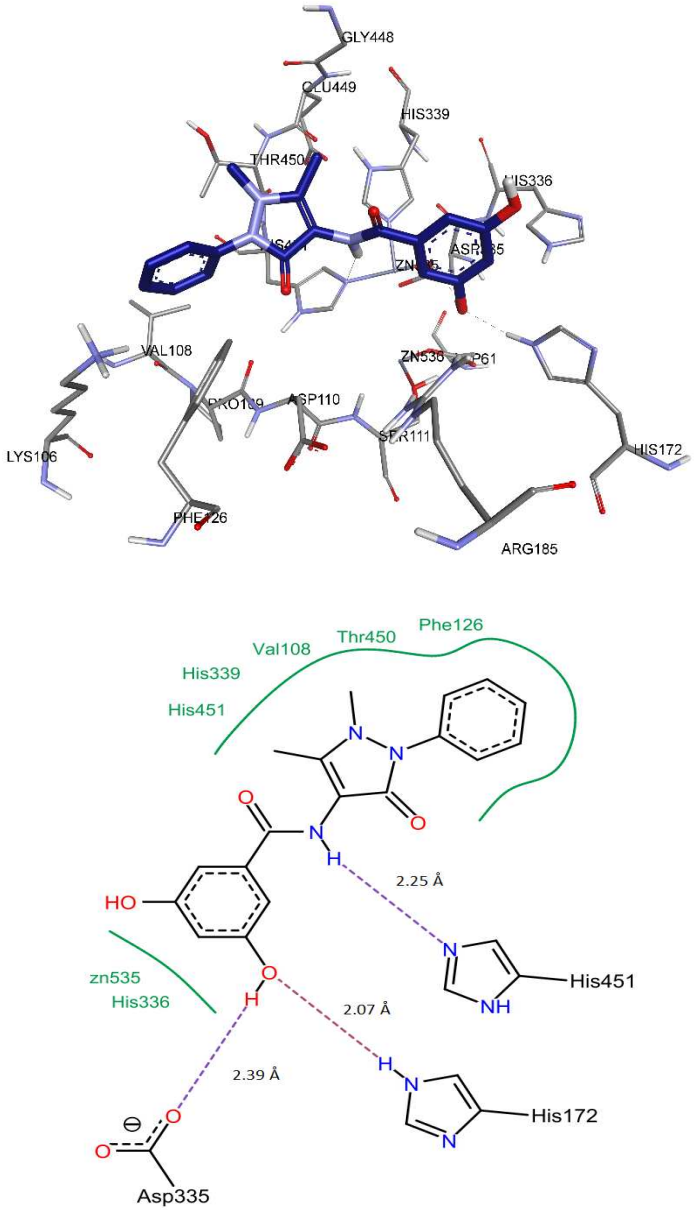

Figure 9. 3D and 2D binding site interactions of **4g.**

Human Placental Alkaline Phosphatase (*h*-PLAP) Docking

Compound **4f** was found to be the most active *h*-PLAP inhibitor, and was therefore selected for molecular docking studies against this enzyme, for which crystal structure is available from the Protein Data Bank (*h*-PLAP, PDB id: 1ZED). No direct binding with the zinc ions was found. Detailed analysis of the docked mode of 4f indicated presence of two hydrogen bonds involving carbonyl oxygen of pyrazole ring and NH of carboxamide group. The carbonyl oxygen of pyrazole ring was found to make a hydrogen with NH of amino acid residue His432 (2.08 Å), while at the same time the nitrogen atom the imidazole ring of same amino acid residue, His432, was making another hydrogen bond (2.31 Å) with the NH of carboxamide group. The 3D and 2D binding site interactions of 4f are given in figures below. The 3D and 2D binding site interactions of **4i** are given in Figure 10.

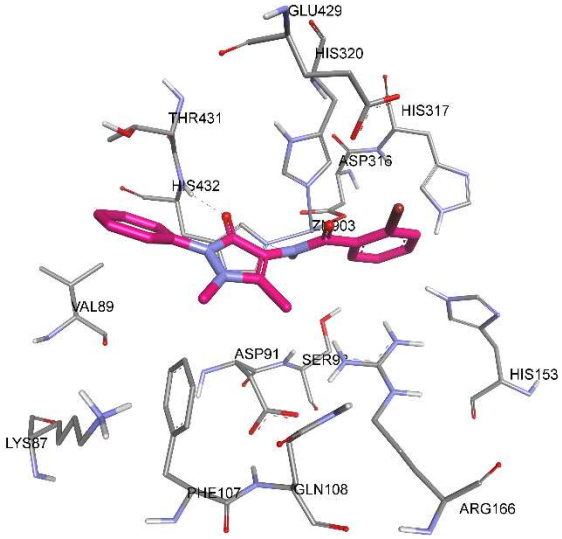

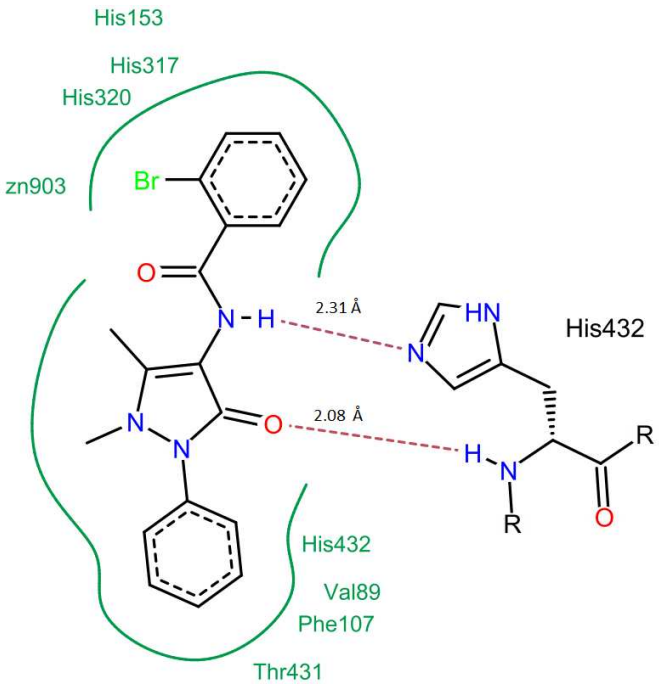

Figure 10. 3D and 2D binding site interactions of **4f.**

Conclusion

We have carried out synthesis, characterization and biological evaluation of some benzamides derivatives of phenazone. The obtained data showed that some of these compounds were potent inhibitors of both APs and e5-NT. The compounds tested against four APs yielded four inhibitors of *h*-GCAP, five inhibitors of *h*-IAP, eight inhibitors of *h*-PLAP and all as inhibitor of *h*-TNAP. Most of the compounds showed more potent inhibition on e5-NT than on APs even at lower concentration. Compunds **4c, 4g, 4h** and **4i** are of great interest as it inhibit e5-NT, which may be used to inhibit totally the production of adenosine from AMP. The new and potent inhibitors can now be used to study the potential e5-NT as a novel drug target.

Acknowledgements

AK and MAH acknowledge the funding from Higher Education Commission (HEC) of Pakistan for NRPU project (No. 1691) and PhD studies, respectively. J. Iqbal is thankful to the Organization for the Prohibition of Chemical Weapons (OPCW), The Hague, The Netherlands and Higher Education Commission of Pakistan for the financial support through Project No. 20-

3733/NRPU/R&D/ 14/520 for the financial support." JS received support from the Canadian Institutes of Health Research (CIHR) and was also a recipient of a “Chercheur National” research award from the *Fonds de recherche du Québec – Santé* (FRQS).

References

1. A. R. Beaudoin, J. Sévigny and M. Picher, *ATPases*, 1996, 5, 369-40l.

2. M. I. Choudhary, N. Fatima, M. A. Abbasi, S. Jalil, V. U. Ahmad and Atta-ur-Rahman, *Bioorg. Med. Chem.,* 2004, 12, 5793-8.

3. E. A. Sergienko and J. L. Millán, *Nat. Protoc.,* 2010, 5, 1431-9.

4. T. Akhtar, S. Hameed, N. A. Al-Masoudi, R. Loddo and P. Colla, *Acta Pharm*., 2008, 58, 135-49.

5. F. Kukulski, S. A. Lévesque, E. G. Lavoie, J. Lecka, F. Bigonnesse, A. F. Knowles, S. C. Robson, T. L. Kirley and J. Sévigny, *Purinergic Signal.,* 2005, 1, 193-204.

6. S. Belli, A. Sali, J. W. Goding, *Biochem J.,* 1994, 304, 75-80.

7. P. Jin-Hua, J. W. Goding, H. Nakamura and K. Sano, *Genomics,* 1997, 45, 412-5.

8. E. F. Pettersen, T. D. Goddard, C. C. Huang, G. S. Couch, D. M. Greenblatt, E. C. Meng and T. E. Ferrin, *J. Comput. Chem.*, 2004, 25, 1605-12.

9. A. Šali and T. L. Blundell, *J. Mol. Biol.,* 1993, 234, 779-815.

10. S. F. Altschul, W. Gish, W. Miller, E. W. Myers and D. J. Lipman, *J. Mol. Biol.*, 1990, 215, 403-10.

11. K. Knapp, M. Zebisch, J. Pippel, A. El-Tayeb, C. E. Müller and N. Sträter, *Structure,* 2012, 20, 2161-73.

12. V. B. Chen, W. B. Arendall, J. J. Headd, D. A. Keedy, R. M. Immormino, G. J. Kapral, L. W. Murray, J. S. Richardson and D. C. Richardson, *Acta Crystallogr. D Biol. Crystallogr.,* 2009, 66, 12-21.

13. A. M. Veselinović, J. B. Milosavljević, A. A. Toropov and G. M. Nikolić, *Arch. Pharm. (Weinheim),* 2013, 346, 134-9.

14. I. Khan, S. J. A. Shah, S. A. Ejaz, A. Ibrar, S. Hameed, J. Lecka, J. L. Millan, J. Sévigny and J. Iqbal, *RSC Adv.*, 2015, 5, 64404-64413.

15. A. Shaabani, E. Soleimani and A. H. Rezayan, *Tetrahedron Lett.,* 2007, 48, 6137-41.

16. M. al-Rashida, J. Iqbal. *Med Res Rev*., 2014, 34, 703-43.

17. M. al-Rashida, J. Iqbal. *Mini Rev Med Chem*. 2015, 15, 41-51.

18. S. Sidique, R. Ardecky, Y. Su, S. Narisawa, B. Brown, JL. Millán, E. Sergienko, ND. Cosford. *Bioorg Med Chem Lett.* 2009, 19, 222-5.

19. Y. Bravo, P. Teriete, R. P. Dhanya, R. Dahl, P. S. Lee, T. Kiffer-Moreira, S. R. Ganji, E. Sergienko, L. H. Smith, C. Farquharson, J. L. Millán and N. D. Cosford, *Bioorg. Med. Chem. Lett.,* 2014, 24, 4308-11.

20. M. M. Bradford, *Anal. Biochem.,* 1976, 72, 248-54.

21. R. Raza, A. Saeed, J. Lecka, J. Sevigny and J. Iqbal, *Med. Chem.,* 2012, 8, 1133-9.

22. E. F. Pettersen, T. D. Goddard, C. C. Huang, G. S. Couch, D. M. Greenblatt, E. C. Meng, T. E. Ferrin, *J. Comput. Chem*. 2004, 25, 1605.

23. A. Šali, T. L. Blundell, *J. Mol. Biol*. 1993, 234, 779.

24. S. F. Altschul, W. Gish, W. Miller, E. W. Myers, D. J. Lipman, *J. Mol. Biol*. 1990, 215, 403.

25. S. B. Needleman, C. D. Wunsch. *J. Mol. Biol*. 1970, 48, 443–53.

26. V. B. Chen, W. B. Arendall 3rd, J. J. Headd, D. A. Keedy, R. M. Immormino, G. J. Kapral, L. W. Murray, J. S. Richardson, D. C. Richardson. *Acta Crystallogr., Sect. D: Biol. Crystallogr*. 2010, 66, 12.

27. K. Knapp, M. Zebisch, J. Pippel, A. El-Tayeb, C. E. Müller, N. Sträter. *Structure*. 2012, 20, 2161-73.

28. ACD/ChemSketch, version 12.01, Advanced Chemistry Development Inc, Toronto, ON, Canada, www.acdlabs.com, 2013.

29. M. A. Thompson. "Molecular docking using ArgusLab, an efficient shape-based search algorithm and AScore scoring function," in Proceedings of the ACS Meeting, Philadelphia, Pa, USA, March-April 2004, 172, CINF 42. [http://www.arguslab.com]

30. http://www.biosolveit.de/LeadIT/.

31. Accelrys Software Inc., Discovery Studio Modeling Environment, Release 4.0, San Diego: Accelrys Software Inc., 2013.

32. M. T. Makhija, R. T. Kasliwal, V. M. Kulkarni and N. Neamati, *Bioorg. Med. Chem.,* 2004, 12, 2317-33.